 CMES, vol.40, no.1, pp.29-62, 2009

A boundary element formulation for incremental nonlinear elastic deformation of compressible solids

Sergia Colli[1], **Massimiliano Gei**[1] **and Davide Bigoni**[1,2]

Abstract: Incremental plane strain deformations superimposed upon a uniformly stressed and deformed nonlinear elastic (compressible) body are treated by developing *ad hoc* boundary integral equations that, discretized, lead to a novel boundary element technique. The approach is a generalization to compressible elasticity of results obtained by Brun, Capuani, and Bigoni (2003, Comput. Methods Appl. Mech. Engrg. 192, 2461-2479), and is based on a Green's function here obtained through the plane-wave expansion method. New expressions for Green's tractions are determined, where singular terms are solved in closed form, a feature permitting the development of a optimized numerical code. An application of the presented formulation, namely, bifurcation of a compressible Mooney-Rivlin rectangular block, highlights the strengths of the approach.

Keywords: Green's function; boundary integral equations; shear bands; bifurcation; instability.

1 Introduction

The presence of prestress strongly influences the incremental response of nonlinear elastic solids, opening the possibility of bifurcations and instabilities (shear bands included), and 'shifting' the natural frequencies of the system towards the low-frequency range. Consequently, the analysis of the incremental problem in nonlinear elasticity becomes important in view of various engineering applications [Stafford, Harrison, Beers, Karim, Amis, Vanlandingham, Kim, Volksen, Miller and Simonyi (2004), Plante and Dubowsky (2006), Michel, Lopez-Pamies, Ponte Castañeda and Triantafyllidis (2007), DeBotton, Tevet-Deree and Socolsky (2007), Bigoni, Gei and Movchan (2008), Gei (2008), Gei, Movchan and Bigoni (2009)].

[1] Department of Mechanical and Structural Engineering, University of Trento, Via Mesiano 77, I-38123, Trento, Italy.

[2] Corresponding author, Tel. +39 0461 882507; Fax: +39 0461 882599; Web-site: http://www.ing.unitn.it/∼bigoni; E-mail: bigoni@ing.unitn.it.

It has been shown in a series of recent papers [Bigoni and Capuani (2002, 2005), Bigoni, Capuani, Bonetti and Colli (2007), Brun, Capuani and Bigoni (2003a, b)] that Green's functions and boundary integral equations can be derived and successfully applied to the solution of incremental problems of nonlinear elasticity. This application becomes, say, 'direct' when the state of prestress and prestrain is uniform[1], but can also be pursued in cases where this is not, employing volume discretization, but without introducing domain integrals as shown by Bertoldi, Brun and Bigoni (2005)[2]. All these results are referred to incompressible elasticity, while ordinary materials are usually compressible. Therefore, the question spontaneously arises whether or not compressible elasticity can also be successfully approached. We provide a positive and definitive answer to this question in the present article, so that, with reference to the general constitutive framework for incremental elasticity proposed by Hill (1979), which describes all possible compressible elastic orthotropic materials, we obtain the following results.

- The Green's functions for incremental displacements, deformations and stresses are derived through the plane wave expansion method [Courant and Hilbert (1962), Gel'fand and Shilov (1964)], within the elliptic regime. Simple formulae are derived in which the singular terms are solved in closed-form. It is shown that these Green's functions reduce in the incompressible case to the corresponding formulae given by Bigoni and Capuani (2002) and Bigoni, Capuani, Bonetti and Colli (2007).

- Following the perturbative approach to material instabilities proposed by Bigoni and Capuani (2002, 2005), shear band formation is analyzed near (but still within) the elliptic boundary for an infinite, compressible material, the so-called 'Kirchhoff-Saint Venant material', thus confirming previous results obtained in the incompressible limit.

- The boundary element technique for incremental elastic boundary value problems proposed by Brun, Capuani and Bigoni (2003a, b) and Bigoni, Ca-

[1] For uniform prestress, the incremental response of a nonlinear elastic material becomes, in a sense, similar to that of an orthotropic elastic solid, for which Green's functions are known [see Vogel and Rizzo (1973), Cruse (1988), Balas, Sladek and Sladek (1989), Mantic and Paris (1998), Gaul, Kögl and Wagner (2003), and Shiah, Lin and Tan (2006)].

[2] The standard approach to boundary elements for nonlinear constitutive equations, as for instance elastoplasticity, is to discretize the domain under consideration to treat the hypersingular integrals connected to the nonlinearity (Swedlow and Cruse, 1971; Mukherjee, 1977; Maier, 1983; Telles, 1983; Sladek and Sladek, 1999; Miers and Telles, 2004). A volume discretization is also needed when the method proposed by Bertoldi, Brun and Bigoni (2005) is employed, but no hypersingular terms arise, so that the method results in a sort of direct applications of techniques for linear anisotropic elasticity.

puani, Bonetti and Colli (2007) is generalized to compressible incremental orthotropic elasticity.

The boundary element formulation derived in the present article has been implemented in a Fortran90 collocation code[3], in which integrations are numerically performed using Gaussian quadrature formulae. In this approach, the proposed boundary element formulation retains the essential advantage that only the boundary of the body is discretized, without introduction of volume terms. The numerical model has been tested addressing the simple problem of shearing of an elastic block (for which the analytical solution is available) and attacking the bifurcation problem of a rectangular compressible Mooney-Rivlin material [Ogden and Roxburgh (1994)], where an excellent agreement has been found with analytical solutions (also derived here and included in Appendix B) and with analyses performed with other commercial codes (ABAQUS).

The paper is organized as follows. After the constitutive framework for incremental elastic deformations superimposed upon a homogeneously, but arbitrarily, deformed elastic material is presented in Section 2, the infinite-body Green's functions for incremental displacements and for incremental displacement gradient and nominal incremental tractions are obtained in Section 3. Boundary integral equations and boundary element discretization are presented in Section 4, while examples are given in Section 5.

2 Incremental constitutive equations for compressible elastic solids

A compressible, elastic body, is considered, homogeneously prestressed under plane-strain conditions, with Cauchy principal stresses σ_1 and σ_2 aligned parallel to the x_1 and x_2 axes, respectively. The incremental constitutive equations may be written in terms of the Jaumann increment of the Kirchhoff stress $\overset{\nabla}{\tau}$ as [see Hill (1979)]

$$\begin{aligned} &\overset{\nabla}{\tau}_{11}=\mu_1 v_{1,1}+\mu_3 v_{2,2}, \qquad \overset{\nabla}{\tau}_{22}=\mu_3 v_{1,1}+\mu_2 v_{2,2}, \\ &\overset{\nabla}{\tau}_{12}=\overset{\nabla}{\tau}_{21}=\mu(v_{1,2}+v_{2,1}), \end{aligned} \tag{1}$$

where a comma denotes partial differentiation and μ, μ_1, μ_2 and μ_3 are instantaneous moduli, depending on the prestress state.

[3] A general-purpose Fortran90 code for two-dimensional incremental and quasi-static deformations of compressible elastic solids, superimposed upon a given uniform prestressed state has been developed at the Solid & Structural Computational Mechanics Laboratory of the University of Trento, whose executable is available on:
http://www.ing.unitn.it/dims/laboratories/comp_solids_structures.php.

In an updated Lagrangian formulation, incremental equilibrium requires, in the absence of body forces, that

$$\dot{t}_{ij,i} = 0, \tag{2}$$

where $\dot{\mathbf{t}}$ is the nominal stress increment (transpose of the first Piola-Kirchhoff stress tensor). Using the relationship between Jaumann increment of Kirchhoff stress and the increment of nominal stress, namely,

$$\dot{t}_{ij} = \overset{\nabla}{\tau}_{ij} - \sigma_{ik} W_{kj} - D_{ik}\sigma_{kj}, \tag{3}$$

where $W_{ij} = (v_{i,j} - v_{j,i})/2$ and $D_{ij} = (v_{i,j} + v_{j,i})/2$ are the spin tensor and the stretching tensor, respectively, and the dimensionless constants

$$k = \frac{\sigma_1 - \sigma_2}{2\mu}, \quad \chi = \frac{\sigma_1 + \sigma_2}{2\mu}, \tag{4}$$

the constitutive equations (1) can be rewritten in terms of tensor $\dot{\mathbf{t}}$ as

$$\begin{aligned} \dot{t}_{11} &= \mu(\bar{a}\, v_{1,1} + \bar{\mu}_3\, v_{2,2}), \quad \dot{t}_{22} = \mu(\bar{\mu}_3\, v_{1,1} + \bar{b}\, v_{2,2}), \\ \dot{t}_{12} &= \mu(\bar{\alpha}\, v_{2,1} + \bar{\gamma} v_{1,2}), \quad \dot{t}_{21} = \mu\,(\bar{\beta} v_{1,2} + \bar{\gamma} v_{2,1}), \end{aligned} \tag{5}$$

where

$$\begin{aligned} &\mu\bar{a} = \mu_1 - \sigma_1, \quad \mu\bar{b} = \mu_2 - \sigma_2, \quad \mu\bar{\mu}_3 = \mu_3, \\ &\bar{\alpha} = 1 + k, \quad \bar{\beta} = 1 - k, \quad \bar{\gamma} = 1 - \chi. \end{aligned} \tag{6}$$

Uniaxial tension (compression) along the x_1-axis corresponds to $\chi = k$ and $k > 0$ ($k < 0$), whereas, along the x_2-axis, uniaxial tension (compression) corresponds to $\chi = -k$ and $k < 0$ ($k > 0$).

For a hyperelastic material, incremental moduli and current Cauchy stress are functions of principal stretches $\lambda_1, \lambda_2, \lambda_3$ ($\lambda_3 = 1$ for plane strain) through the strain-energy function $W(\lambda_1, \lambda_2, \lambda_3)$, in the following form

$$\begin{aligned} \mu_1 = \frac{1}{\lambda_2}\left(\lambda_1 \frac{\partial^2 W}{\partial \lambda_1^2} + \frac{\partial W}{\partial \lambda_1}\right), \quad \mu_2 = \frac{1}{\lambda_1}\left(\lambda_2 \frac{\partial^2 W}{\partial \lambda_2^2} + \frac{\partial W}{\partial \lambda_2}\right), \quad \mu_3 = \frac{\partial^2 W}{\partial \lambda_1 \partial \lambda_2}, \\ \mu = \frac{\sigma_1 - \sigma_2}{2}\frac{\lambda_1^2 + \lambda_2^2}{\lambda_1^2 - \lambda_2^2}, \quad \sigma_1 = \frac{1}{\lambda_2}\frac{\partial W}{\partial \lambda_1}, \quad \sigma_2 = \frac{1}{\lambda_1}\frac{\partial W}{\partial \lambda_2}. \end{aligned} \tag{7}$$

From eqn. $(7)_4$ we obtain

$$k = \frac{\lambda_1^2 - \lambda_2^2}{\lambda_1^2 + \lambda_2^2}, \tag{8}$$

regardless of the form of the strain-energy function.

2.1 The classification of regimes

The substitution of eqns. (5) and (4) into eqn. (2) provides a system of coupled partial differential equations

$$\begin{cases} \bar{a}v_{1,11} + (\bar{\mu}_3 + \bar{\gamma})v_{2,12} + \bar{\beta}v_{1,22} = 0, \\ \\ \bar{b}v_{2,22} + (\bar{\mu}_3 + \bar{\gamma})v_{1,21} + \bar{\alpha}v_{2,11} = 0. \end{cases} \tag{9}$$

Hill (1979) has classified the general solutions of (9) in the form

$$v_i = V_i\, f(\rho x_1 + x_2) \quad (i = 1,2), \tag{10}$$

where f is a twice differentiable function, V_1, V_2 are constant amplitudes and ρ satisfies the characteristic equation

$$\bar{a}\bar{\alpha}\rho^4 + \bar{d}\rho^2 + \bar{b}\bar{\beta} = 0, \tag{11}$$

where

$$\bar{d} = \bar{a}\bar{b} + \bar{\alpha}\bar{\beta} - (\bar{\mu}_3 + \bar{\gamma})^2. \tag{12}$$

The regime of the system of differential eqns. (9) depends on the nature of solutions to eqn. (11), namely

$$\left.\begin{matrix} \rho_+^2 \\ \rho_-^2 \end{matrix}\right\} = \frac{-\bar{d} \pm \sqrt{\bar{d}^2 - 4\bar{a}\bar{b}\bar{\alpha}\bar{\beta}}}{2\bar{a}\bar{\alpha}}. \tag{13}$$

In particular, the elliptic complex (EC) regime corresponds to four complex conjugate roots ρ, so that

$$|\bar{d}| < 2\sqrt{\bar{a}\bar{b}\bar{\alpha}\bar{\beta}} \quad \text{and} \quad \bar{a}\bar{b}\bar{\alpha}\bar{\beta} > 0. \tag{14}$$

In the elliptic imaginary (EI) regime the four solutions (13) are all pure imaginary. The involved parameters satisfy either

$$|\bar{d}| > 2\sqrt{\bar{a}\bar{b}\bar{\alpha}\bar{\beta}} \quad \text{and} \quad \bar{a}\bar{\alpha} > 0,\ \ \bar{b}\bar{\beta} > 0, \tag{15}$$

or

$$|\bar{d}| < -2\sqrt{\bar{a}\bar{b}\bar{\alpha}\bar{\beta}} \quad \text{and} \quad \bar{a}\bar{\alpha} < 0,\ \ \bar{b}\bar{\beta} < 0. \tag{16}$$

In the Hyperbolic (H) regime eqn. (11) admits four real and distinct solutions, so that $\bar{d}$ must satisfy

$$|\bar{d}| > 2\sqrt{\bar{a}\bar{b}\bar{\alpha}\bar{\beta}}, \tag{17}$$

together with either

$$\bar{a}\bar{\alpha} > 0,\ \bar{b}\bar{\beta} > 0,\ \bar{d} < 0 \quad \text{or} \quad \bar{a}\bar{\alpha} < 0,\ \bar{b}\bar{\beta} < 0,\ \bar{d} > 0. \tag{18}$$

In the Parabolic (P) regime there are two real and two imaginary roots, a situation occurring when

$$\bar{a}\bar{b}\bar{\alpha}\bar{\beta} < 0. \tag{19}$$

The classification of regimes can be graphically represented in the three-dimensional space spanned by variables $X = \bar{a}\bar{b} - \bar{\alpha}\bar{\beta}$, $Y = (\bar{\mu}_3 + \bar{\gamma})^2$ and $Z = \bar{a}\bar{b} + \bar{\alpha}\bar{\beta}$. The vanishing of the discriminant in condition (13), namely $\bar{d}^2 - 4\bar{a}\bar{b}\bar{\alpha}\bar{\beta} = 0$ or, $X^2 + Y^2 - 2ZY = 0$, describes the surface of a cone in that space with the vertex in the origin and the axis described by equations $X = 0$ and $Y = Z$. The cone has circular section at constant Z. The region inside the cone corresponds to the EC regime, while the regions corresponding to the other regimes can be inferred from the $X/Z - Y/Z$ plane representation of Fig. 1.

Simple models of compressible elasticity will be presented below to be employed in the numerical applications deferred to Section 5.

2.2 Limit of incompressibility and isotropic elasticity

The compressible constitutive equations (5) yield the incompressible constitutive framework given by Biot (1965) in the limit $\{\mu_1, \mu_2, \mu_3\} \longrightarrow \infty$, but with their differences [i.e. $\mu_i - \mu_k\ (i \neq k)$] remaining bounded, yielding

$$4\mu^* = \mu_1 + \mu_2 - 2\mu_3 + \sigma_1 + \sigma_2, \tag{20}$$

where μ^* is an incremental modulus which, together with μ, governs the in-plane incompressible response, and depends on the current state.

In the unstressed state (in other words, in the infinitesimal theory) $\overset{\nabla}{\tau}$ coincides with the Cauchy stress and, for isotropic materials, the incremental moduli become functions of the Young modulus E and Poisson's ratio ν as

$$\mu_1 = \mu_2 = \frac{(1-\nu)E}{(1+\nu)(1-2\nu)}, \quad \mu_3 = \frac{\nu E}{(1+\nu)(1-2\nu)}, \quad \mu = \frac{E}{2(1+\nu)}. \tag{21}$$

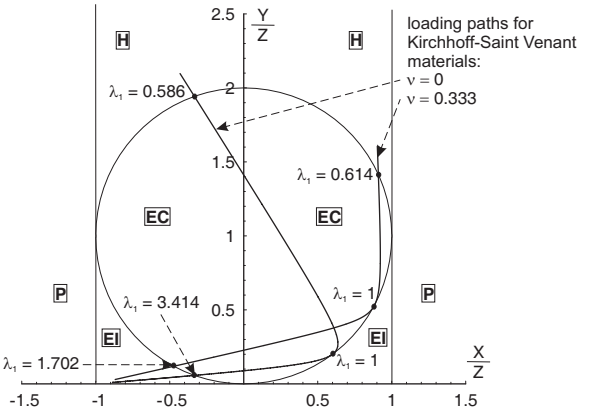

Figure 1: Graphical representation of the classification of regimes of equilibrium [eqns. (9)] in the $X/Z-Y/Z$ plane ($X=\bar{a}\bar{b}-\bar{\alpha}\bar{\beta}$, $Y=(\bar{\mu}_3+\bar{\gamma})^2$, $Z=\bar{a}\bar{b}+\bar{\alpha}\bar{\beta}$). EI denotes the elliptic imaginary regime, EC the elliptic complex regime, H the hyperbolic regime, and P the parabolic regime. The paths followed in this plane during plane-strain uniaxial tension/compression of two Kirchhoff–Saint Venant elastic materials ($\lambda_0=\nu=0$, and $\lambda_0/\mu_0=2$ corresponding to $\nu=0.333$) are also reported.

2.3 Kirchhoff-Saint Venant material

The Kirchhoff-Saint Venant model has well-known limitations[4] [see for instance Ciarlet (1988)], but adds to the merit of a great simplicity the capability of correctly capturing a number of bifurcations in structures. For this material model, the energy function takes the simple form

$$W=\frac{\lambda_0}{2}(\mathrm{tr}\mathbf{E}^{(2)})^2+\mu_0\,\mathbf{E}^{(2)}\cdot\mathbf{E}^{(2)}, \tag{22}$$

[4] Under plane-strain conditions, the tensile branch of the uniaxial true stress–longitudinal stretch law exhibits a limit stretch –where the stress becomes unbounded– at

$$\lambda_1^t=\sqrt{\frac{2(\mu_0+\lambda_0)}{\lambda_0}},$$

whereas, in compression, the true stress reaches a maximum loading at

$$\lambda_1^c=\sqrt{\frac{3}{2}+\frac{3\mu_0}{2\lambda_0}-\frac{\sqrt{9\mu_0^2+14\lambda_0\mu_0+5\lambda_0^2}}{2\lambda_0}}.$$

where $\mathbf{E}^{(2)}$ denotes the Green-Lagrange strain tensor and λ_0 and μ_0 are constants playing the same role of the Lamé constants within the infinitesimal theory, so that a Poisson's ratio can be defined by $\nu = \lambda_0/[2(\lambda_0+\mu_0)]$. Differentiation of W with respect to $\mathbf{E}^{(2)}$ yields the second Piola-Kirchhoff stress $\mathbf{T}^{(2)}$, in the following form

$$\mathbf{T}^{(2)} = \lambda_0(\mathrm{tr}\mathbf{E}^{(2)})\mathbf{I} + 2\mu_0\mathbf{E}^{(2)}, \tag{23}$$

akin to the constitutive equations of the infinitesimal elasticity theory. The incremental moduli can be readily calculated employing eqns. (7).

The classification of regimes for this material is illustrated in Fig. 1, where the paths followed by two different materials (corresponding to Poisson's ratios equal to 0 and 0.333) during a monotonic loading starting at $\lambda_1 = 1$, and corresponding to uniaxial tension and compression are reported. In these conditions of plane strain uniaxial stress, loss of ellipticity at the EC/H border always occurs under compressive stress before λ_1^c is reached, while under tensile stress the regime remains always elliptic.

2.4 Compressible Mooney-Rivlin material

A strain-energy function will be used in the examples, based on the splitting between isovolumetric and pure volumetric response as

$$W(\lambda_1,\lambda_2,\lambda_3) = W_{\mathrm{iso}}(\bar{\lambda}_1,\bar{\lambda}_2,\bar{\lambda}_3) + W_{\mathrm{vol}}(J), \tag{24}$$

where

$$J = \lambda_1\lambda_2\lambda_3, \tag{25}$$

and $\bar{\lambda}_i = J^{-1/3}\lambda_i$ $(i = 1,2,3)$ are the modified principal stretches. In particular, a Mooney-Rivlin strain-energy potential is adopted, which, in terms of the strain invariants $\bar{I}_1$ and $\bar{I}_2$, is expressed by

$$W = c_1(\bar{I}_1 - 3) + c_2(\bar{I}_2 - 3) + \frac{1}{c_3}(J-1)^2, \tag{26}$$

where c_1, c_2 and c_3 are constitutive parameters expressed in terms of the initial shear modulus μ_0 and initial bulk modulus q_0 as

$$\mu_0 = 2(c_1+c_2), \quad q_0 = \frac{2}{c_3}, \tag{27}$$

and $\bar{I}_1$ and $\bar{I}_2$ are expressed in terms of the deviatoric stretches $\bar{\lambda}_i = J^{-1/3}\lambda_i$ as

$$\begin{aligned} \bar{I}_1 &= \bar{\lambda}_1^2 + \bar{\lambda}_2^2 + \bar{\lambda}_3^2 = I_1(\mathbf{B})J^{-2/3}, \\ \bar{I}_2 &= \bar{\lambda}_1^{-2} + \bar{\lambda}_2^{-2} + \bar{\lambda}_3^{-2} = I_2(\mathbf{B})J^{-4/3}, \end{aligned} \tag{28}$$

where $I_1(\mathbf{B})$ and $I_2(\mathbf{B})$ denote the principal invariants of the left Cauchy-Green strain tensor $\mathbf{B}$

$$I_1(\mathbf{B}) = \mathrm{tr}\mathbf{B}, \quad I_2(\mathbf{B}) = \frac{1}{2}\left(I_1^2 - \mathrm{tr}\mathbf{B}^2\right). \tag{29}$$

The relevant incremental moduli can be calculated through eqns. (7). It can be shown that this material remains always in the elliptic imaginary regime. Being a compressible material, it is worth mentioning that the Poisson's ratio for this material becomes

$$\nu = 1 - \frac{3 + 2\mu_0 c_3}{6 + \mu_0 c_3}. \tag{30}$$

3 The quasi-static Green's function

The quasi-static, infinite-body Green's function for a compressible, elastic material subject to a homogenous prestress state can be obtained as the solution of eqns. (9) when a unit point force is applied

$$\dot{f}_j^g = \delta_{jg}\delta(\mathbf{x}), \tag{31}$$

acting at the axes origin $\mathbf{x} = \mathbf{0}$, where $\delta(\mathbf{x})$ is the two-dimensional Dirac delta function. The solution is obtained by employing a plane wave expansion method [Courant and Hilbert (1962), Gel'fand and Shilov (1964)] for which a generic function $h(\mathbf{x})$ can be written as

$$h(\mathbf{x}) = -\frac{1}{4\pi^2}\oint_{|\boldsymbol{\omega}|=1} \tilde{h}(\boldsymbol{\omega}\cdot\mathbf{x})d\omega, \tag{32}$$

where $\boldsymbol{\omega}$ is the radial unit vector centered at the origin of the position vector $\mathbf{x}$ (Fig. 2) and $\tilde{h}$ is the transformed function. Noting that the transformed function $\tilde{\delta}$ of the Dirac delta is $\tilde{\delta}(\boldsymbol{\omega}\cdot\mathbf{x}) = 1/(\boldsymbol{\omega}\cdot\mathbf{x})^2$, equilibrium equations in the transformed domain are [see the derivation in Bertoldi, Brun and Bigoni (2005)]

$$A_{ik}(\boldsymbol{\omega})\,\tilde{v}_k^{g\prime\prime}(\boldsymbol{\omega}\cdot\mathbf{x}) + \delta_{ig}\tilde{\delta} = 0, \tag{33}$$

where A_{ik} is the acoustic tensor associated with the constitutive eqns. (5) and a prime denotes differentiation with respect to the argument $\boldsymbol{\omega}\cdot\mathbf{x}$. Henceforth, our attention will be focused on the elliptic regime (EI or EC) in which the acoustic tensor is not singular, and where the solution to eqn. (33) is

$$\tilde{v}_i^g(\boldsymbol{\omega}\cdot\mathbf{x}) = (A^{-1})_{ig}\log|\boldsymbol{\omega}\cdot\bar{\mathbf{x}}|, \tag{34}$$

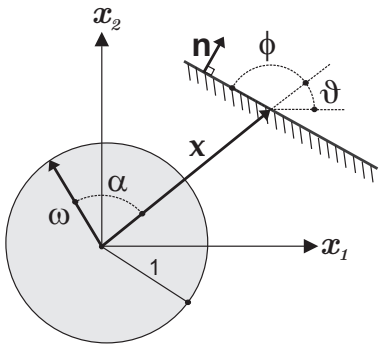

Figure 2: Reference system, vectors $\boldsymbol{\omega}$, $\mathbf{x}$, $\mathbf{n}$, and angles θ, α and ϕ.

where $\bar{\mathbf{x}}$ is a dimensionless measure of $\mathbf{x}$. The Green's function can now be obtained by antitransforming eqn. (34)

$$v_i^g(\mathbf{x}) = -\frac{1}{4\pi^2} \oint_{|\boldsymbol{\omega}|=1} (A^{-1})_{ig} \log|\boldsymbol{\omega}\cdot\bar{\mathbf{x}}|\, d\omega. \tag{35}$$

Introducing the radial measure of the distance $\bar{r} = |\bar{\mathbf{x}}|$ and the angle α between $\boldsymbol{\omega}$ and $\mathbf{x}$ (Fig. 2), the Green's function for incremental displacement satisfying eqns. (9) can be expressed as

$$v_i^g(\mathbf{x}) = -\frac{\log\bar{r}}{4\pi^2} \int_0^{2\pi} (A^{-1})_{ig}\, d\alpha - \frac{1}{4\pi^2} \int_0^{2\pi} (A^{-1})_{ig} \log|\cos\alpha|\, d\alpha. \tag{36}$$

3.1 The incremental displacements

The components of the acoustic tensor $\mathbf{A}(\boldsymbol{\omega})$ appearing in eqn. (33) for the constitutive eqns. (5) are

$$A_{11} = \mu(\bar{a}\omega_1^2 + \bar{\beta}\omega_2^2), \quad A_{22} = \mu(\bar{\alpha}\omega_1^2 + \bar{b}\omega_2^2), \tag{37}$$

$$A_{12} = A_{21} = \mu(\bar{\mu}_3 + \bar{\gamma})\omega_1\omega_2.$$

The determinant of the acoustic tensor (37) is $\mu^2\Lambda(\alpha+\theta)$, where

$$\Lambda(\alpha+\theta) = \bar{a}\bar{\alpha}\sin^4(\alpha+\theta)\,[\cot^2(\alpha+\theta) - \rho_+^2][\cot^2(\alpha+\theta) - \rho_-^2], \tag{38}$$

in which $\alpha+\theta = \arctan(\omega_2/\omega_1)$ and ω_1 and ω_2 are the components of the vector $\boldsymbol{\omega}$ along the x_1 and x_2 axes.

Note that $\Lambda(\alpha+\theta)$ is always different from zero in the elliptic regime and

$$\Lambda(0)=\Lambda(\pi)=\bar{a}\bar{\alpha},\quad \Lambda(\pi/2)=\Lambda(3\pi/2)=\bar{b}\bar{\beta}. \tag{39}$$

Employing eqn. (36), with the inverse of the acoustic tensor (37), the Green's function in nondimensional polar coordinates $\bar{r}$ and θ becomes

$$\begin{aligned}
v_1^1 &= -\frac{1}{2\pi\mu\bar{a}}\left(\eta_1-\frac{\bar{b}}{\bar{\alpha}}\eta_2\right)\log\bar{r}\\
&\quad -\frac{1}{2\pi^2\mu}\int_0^\pi \frac{\bar{\alpha}\cos^2(\alpha+\theta)+\bar{b}\sin^2(\alpha+\theta)}{\Lambda(\alpha+\theta)}\log|\cos\alpha|\,d\alpha,\\
v_2^2 &= -\frac{1}{2\pi\mu\bar{\alpha}}\left(\eta_1-\frac{\bar{\beta}}{\bar{a}}\eta_2\right)\log\bar{r}\\
&\quad -\frac{1}{2\pi^2\mu}\int_0^\pi \frac{\bar{a}\cos^2(\alpha+\theta)+\bar{\beta}\sin^2(\alpha+\theta)}{\Lambda(\alpha+\theta)}\log|\cos\alpha|d\alpha,\\
v_1^2 &= v_2^1=\frac{\bar{\mu}_3+\bar{\gamma}}{2\pi^2\mu}\int_0^\pi \frac{\sin(\alpha+\theta)\cos(\alpha+\theta)}{\Lambda(\alpha+\theta)}\log|\cos\alpha|\,d\alpha,
\end{aligned} \tag{40}$$

where

$$\eta_1=\frac{1}{\sqrt{-\rho_+^2}+\sqrt{-\rho_-^2}},\quad \eta_2=\frac{1}{\rho_-^2\sqrt{-\rho_+^2}+\rho_+^2\sqrt{-\rho_-^2}}. \tag{41}$$

Note that the terms multiplying $\log\bar{r}$ in eqns. (40) are all independent of θ and have been solved explicitly; moreover, all remaining functions of α are π–periodic.

3.2 The gradient of incremental displacements

The gradient of incremental displacements is necessary for the formulation of the boundary element technique and can be obtained *either* directly from eqns. (40), employing the rule

$$\frac{\partial v_i^g}{\partial x_1}=\cos\theta\frac{\partial v_i^g}{\partial r}-\frac{\sin\theta}{r}\frac{\partial v_i^g}{\partial\theta},\qquad \frac{\partial v_i^g}{\partial x_2}=\sin\theta\frac{\partial v_i^g}{\partial r}+\frac{\cos\theta}{r}\frac{\partial v_i^g}{\partial\theta}, \tag{42}$$

where $r=|\mathbf{x}|$, *or* by differentiation and subsequent transformation of $\tilde{\mathbf{v}}^g$ as

$$v_{i,k}^g=-\frac{1}{4\pi^2}\oint_{|\boldsymbol{\omega}|=1}\tilde{v}_{i,k}^g(\boldsymbol{\omega}\cdot\mathbf{x})d\omega. \tag{43}$$

By application of the chain rule, it turns out that the spatial gradient of a generic function $\tilde{h}$ in the transformed domain writes as

$$\operatorname{grad}\tilde{h} = \tilde{h}'(\boldsymbol{\omega}\cdot\mathbf{x})\boldsymbol{\omega}, \tag{44}$$

so that, from (34), we obtain

$$\tilde{v}^g_{i,k} = (A^{-1})_{ig}\,\omega_k. \tag{45}$$

In *both cases* the result remains the same, namely,

$$\begin{aligned}
v^1_{1,1} &= -\frac{\cos\theta}{2\pi r\mu\bar{a}}\left(\eta_1 - \frac{\bar{b}}{\bar{\alpha}}\eta_2\right) + \frac{\sin\theta}{2\pi^2 r\mu}\int_0^\pi \zeta_1(\alpha+\theta)\log|\cos\alpha|\,d\alpha,\\
v^1_{1,2} &= -\frac{\sin\theta}{2\pi r\mu\bar{a}}\left(\eta_1 - \frac{\bar{b}}{\bar{\alpha}}\eta_2\right) - \frac{\cos\theta}{2\pi^2 r\mu}\int_0^\pi \zeta_1(\alpha+\theta)\log|\cos\alpha|\,d\alpha,\\
v^1_{2,1} &= -\frac{\sin\theta}{2\pi^2 r\mu}\int_0^\pi \zeta_2(\alpha+\theta)\log|\cos\alpha|\,d\alpha,\\
v^1_{2,2} &= \frac{\cos\theta}{2\pi^2 r\mu}\int_0^\pi \zeta_2(\alpha+\theta)\log|\cos\alpha|\,d\alpha,
\end{aligned} \tag{46}$$

for $g=1$, and

$$\begin{aligned}
v^2_{1,1} &= v^1_{2,1}, \quad v^2_{1,2} = v^1_{2,2},\\
v^2_{2,1} &= -\frac{\cos\theta}{2\pi r\mu\bar{\alpha}}\left(\eta_1 - \frac{\bar{\beta}}{\bar{a}}\eta_2\right) + \frac{\sin\theta}{2\pi^2 r\mu}\int_0^\pi \zeta_3(\alpha+\theta)\log|\cos\alpha|\,d\alpha,\\
v^2_{2,2} &= -\frac{\sin\theta}{2\pi r\mu\bar{\alpha}}\left(\eta_1 - \frac{\bar{\beta}}{\bar{a}}\eta_2\right) - \frac{\cos\theta}{2\pi^2 r\mu}\int_0^\pi \zeta_3(\alpha+\theta)\log|\cos\alpha|\,d\alpha,
\end{aligned} \tag{47}$$

for $g=2$, where functions $\zeta_i(\xi)$ $(i=1,2,3)$ are given by

$$\begin{aligned}
\zeta_1(\xi) &= \frac{\Lambda(\xi)(\bar{b}-\bar{\alpha})\sin 2\xi - \Lambda'(\xi)(\bar{\alpha}\cos^2\xi + \bar{b}\sin^2\xi)}{\Lambda^2(\xi)},\\
\zeta_2(\xi) &= \frac{(\bar{\mu}_3+\bar{\gamma})(\Lambda(\xi)\cos 2\xi - \Lambda'(\xi)\sin\xi\cos\xi)}{\Lambda^2(\xi)},\\
\zeta_3(\xi) &= \frac{\Lambda(\xi)(\bar{\beta}-\bar{a})\sin 2\xi - \Lambda'(\xi)(\bar{a}\cos^2\xi + \bar{\beta}\sin^2\xi)}{\Lambda^2(\xi)},
\end{aligned} \tag{48}$$

with $\Lambda'(\xi) = d\Lambda(\xi)/d\xi$.

3.3 The nominal incremental stresses

The Green's functions for incremental nominal stresses can now be obtained using the Green's functions for the gradient of incremental displacements (46) and (47) into the constitutive laws (5) as

$$\begin{aligned} i^g_{11} &= \mu(\bar{a}\, v^g_{1,1} + \bar{\mu}_3\, v^g_{2,2}), \quad i^g_{22} = \mu(\bar{\mu}_3\, v^g_{1,1} + \bar{b}\, v^g_{2,2}), \\ i^g_{12} &= \mu(\bar{\alpha}\, v^g_{2,1} + \bar{\gamma} v^g_{1,2}), \quad i^g_{21} = \mu(\bar{\beta} v^g_{1,2} + \bar{\gamma} v^g_{2,1}). \end{aligned} \tag{49}$$

3.4 The quasi-static tractions

Although the Green's functions for incremental applied nominal tractions τ^g_j at a boundary of unit outward normal $\mathbf{n}$ can be evaluated through substitution of eqns. (5) into

$$\tau^g_j = i^g_{ij} n_i, \tag{50}$$

an alternative derivation has been suggested by Bigoni, Capuani, Bonetti and Colli (2007). The alternative will now be followed, since it has the merit that it leads to formulae more explicit than those that can be directly achieved from eqn. (50). We operate, in particular, employing the plane wave expansion of nominal traction

$$\tau^g_j(\mathbf{x}) = -\frac{1}{4\pi^2} \oint_{|\boldsymbol{\omega}|=1} \tilde{\tau}^g_j(\boldsymbol{\omega}\cdot\mathbf{x}) d\omega, \tag{51}$$

where

$$\begin{aligned} \tilde{\tau}^1_1 &= \frac{1}{\boldsymbol{\omega}\cdot\mathbf{x}} \left\{ \frac{n_1}{\omega_1} - \frac{n_1\omega_2 - n_2\omega_1}{\Lambda(\boldsymbol{\omega})} \left[\bar{b}\bar{\beta}\frac{\omega_2}{\omega_1} - \{\bar{\gamma}(\bar{\mu}_3 + \bar{\gamma}) + \bar{\beta}(\bar{b} - \bar{\alpha})\}\omega_1\omega_2 \right] \right\}, \\ [5mm]\tilde{\tau}^2_2 &= \frac{1}{\boldsymbol{\omega}\cdot\mathbf{x}} \left\{ \frac{n_2}{\omega_2} + \frac{n_1\omega_2 - n_2\omega_1}{\Lambda(\boldsymbol{\omega})} \left[\bar{a}\bar{\alpha}\frac{\omega_2}{\omega_1} - \{\bar{\gamma}(\bar{\mu}_3 + \bar{\gamma}) + \bar{\alpha}(\bar{a} - \bar{\beta})\}\omega_1\omega_2 \right] \right\}, \\ [5mm]\tilde{\tau}^1_2 &= \frac{1}{\boldsymbol{\omega}\cdot\mathbf{x}} \frac{n_1\omega_2 - n_2\omega_1}{\Lambda(\boldsymbol{\omega})} (\bar{\gamma}\bar{b}\omega_2^2 - \bar{\mu}_3\bar{\alpha}\omega_1^2), \\ [5mm]\tilde{\tau}^2_1 &= \frac{1}{\boldsymbol{\omega}\cdot\mathbf{x}} \frac{n_1\omega_2 - n_2\omega_1}{\Lambda(\boldsymbol{\omega})} (\bar{\mu}_3\bar{\beta}\omega_2^2 - \bar{\gamma}\bar{a}\omega_1^2). \end{aligned} \tag{52}$$

Assuming that the normal to the material surface, to which the traction is referred, can be expressed in terms of the angle ϕ measured from θ (see Fig. 2) as

$$n_1 = \sin(\phi + \theta), \quad n_2 = -\cos(\phi + \theta), \tag{53}$$

the tractions (52) become (see Appendix A)

$$\begin{aligned}
\tau_1^1 &= \frac{\sin\phi}{2\pi^2 r}\left\{\bar{b}\bar{\beta}\oint_0^\pi \frac{\tan\alpha\tan(\alpha+\theta)}{\Lambda(\alpha+\theta)}d\alpha\right. \\
&\left.-[\bar{\gamma}(\bar{\mu}_3+\bar{\gamma})+\bar{\beta}(\bar{b}-\bar{\alpha})]\oint_0^\pi \frac{\tan\alpha\sin(\alpha+\theta)\cos(\alpha+\theta)}{\Lambda(\alpha+\theta)}\,d\alpha\right\}, \\
\tau_2^2 &= -\frac{\sin\phi}{2\pi^2 r}\left\{\bar{a}\bar{\alpha}\oint_0^\pi \frac{\tan\alpha\cot(\alpha+\theta)}{\Lambda(\alpha+\theta)}d\alpha\right. \\
&\left.-[\bar{\gamma}(\bar{\mu}_3+\bar{\gamma})+\bar{\alpha}(\bar{a}-\bar{\beta})]\oint_0^\pi \frac{\tan\alpha\sin(\alpha+\theta)\cos(\alpha+\theta)}{\Lambda(\alpha+\theta)}\,d\alpha\right\}, \\
\tau_2^1 &= \frac{\sin\phi}{2\pi^2 r}\oint_0^\pi \frac{\tan\alpha}{\Lambda(\alpha+\theta)}[\bar{\mu}_3\bar{\alpha}\cos^2(\alpha+\theta)-\bar{\gamma}\bar{b}\sin^2(\alpha+\theta)]\,d\alpha \\
&+\frac{\cos\phi}{2\pi r\bar{a}}\left(\bar{\mu}_3\eta_1+\frac{\bar{\gamma}\bar{b}}{\bar{\alpha}}\eta_2\right), \\
\tau_1^2 &= \frac{\sin\phi}{2\pi^2 r}\oint_0^\pi \frac{\tan\alpha}{\Lambda(\alpha+\theta)}[\bar{\gamma}\bar{a}\cos^2(\alpha+\theta)-\bar{\mu}_3\bar{\beta}\sin^2(\alpha+\theta)]\,d\alpha \\
&+\frac{\cos\phi}{2\pi r\bar{\alpha}}\left(\bar{\gamma}\eta_1+\frac{\bar{\mu}_3\bar{\beta}}{\bar{a}}\eta_2\right).
\end{aligned} \tag{54}$$

Expressions (53) are singular for $\theta=\pi/2$, but can be regularized by applying the rule

$$\oint_a^b f(x)g(x)dx=\int_a^b [f(x)-f(x_0)]g(x)dx+f(x_0)\int_a^b g(x)dx, \tag{55}$$

where function $g(x)$ is singular at $x_0\in[a,b]$, while function $f(x)$ remains regular everywhere in $[a,b]$. Furthermore, the following Cauchy principal values can be calculated

$$\oint_0^\pi \frac{d\alpha}{\pi/2-\alpha}=0, \quad \oint_0^\pi \frac{d\alpha}{\beta-\alpha}=\log\left|\frac{\beta}{\beta-\pi}\right|. \tag{56}$$

In detail, assuming $0 \leq \theta \leq 2\pi$, expressions (54) become

$$\tau_1^1 = \frac{\sin\phi}{2\pi^2 r} \times \left\{ \bar{b}\bar{\beta} \left[\int_0^\pi \left(\frac{\tan\alpha \tan(\alpha+\theta)}{\Lambda(\alpha+\theta)} + \frac{\cot\theta}{\Lambda(\pi/2+\theta)\cos\alpha} - \frac{\cot\theta}{\Lambda(\pi/2)(\beta_1-\alpha)} \right) d\alpha + \frac{\cot\theta}{\Lambda(\pi/2)} \log\left| \frac{\beta_1}{\beta_1-\pi} \right| \right] - [\bar{\gamma}(\bar{\mu}_3+\bar{\gamma}) + \bar{\beta}(\bar{b}-\bar{\alpha})] \int_0^\pi \left(\frac{\tan\alpha \sin(\alpha+\theta)\cos(\alpha+\theta)}{\Lambda(\alpha+\theta)} + \frac{\sin\theta\cos\theta}{\Lambda(\pi/2+\theta)\cos\alpha} \right) d\alpha \right\},$$

$$\tau_2^2 = -\frac{\sin\phi}{2\pi^2 r} \times \left\{ \bar{a}\bar{\alpha} \left[\int_0^\pi \left(\frac{\tan\alpha \cot(\alpha+\theta)}{\Lambda(\alpha+\theta)} + \frac{\tan\theta}{\Lambda(\pi/2+\theta)\cos\alpha} - \frac{\tan\theta}{\Lambda(\pi)(\beta_2-\alpha)} \right) d\alpha + \frac{\tan\theta}{\Lambda(\pi)} \log\left| \frac{\beta_2}{\beta_2-\pi} \right| \right] - [\bar{\gamma}(\bar{\mu}_3+\bar{\gamma}) + \bar{\alpha}(\bar{a}-\bar{\beta})] \int_0^\pi \left(\frac{\tan\alpha \sin(\alpha+\theta)\cos(\alpha+\theta)}{\Lambda(\alpha+\theta)} - \frac{\sin\theta\cos\theta}{\Lambda(\pi/2+\theta)\cos\alpha} \right) d\alpha \right\},$$

$$\tau_2^1 = -\frac{\sin\phi}{2\pi^2 r} \times \int_0^\pi \left(\frac{\tan\alpha[\bar{\gamma}\bar{b}\sin^2(\alpha+\theta) - \bar{\mu}_3\bar{\alpha}\cos^2(\alpha+\theta)]}{\Lambda(\alpha+\theta)} - \frac{\bar{\gamma}\bar{b}\cos^2\theta - \bar{\mu}_3\bar{\alpha}\sin^2\theta}{\Lambda(\pi/2+\theta)\cos\alpha} \right) d\alpha + \frac{\cos\phi}{2\pi r\bar{a}} \left(\bar{\mu}_3\eta_1 + \frac{\bar{\gamma}\bar{b}}{\bar{\alpha}}\eta_2 \right),$$

$$\tau_1^2 = -\frac{\sin\phi}{2\pi^2 r} \times \int_0^\pi \left(\frac{\tan\alpha[\bar{\mu}_3\bar{\beta}\sin^2(\alpha+\theta) - \bar{\gamma}\bar{a}\cos^2(\alpha+\theta)]}{\Lambda(\alpha+\theta)} - \frac{\bar{\mu}_3\bar{\beta}\cos^2\theta - \bar{\gamma}\bar{a}\sin^2\theta}{\Lambda(\pi/2+\theta)\cos\alpha} \right) d\alpha + \frac{\cos\phi}{2\pi r\bar{\alpha}} \left(\bar{\gamma}\eta_1 + \frac{\bar{\mu}_3\bar{\beta}}{\bar{a}}\eta_2 \right), \quad (57)$$

with angles β_1, β_2 defined as

$$\beta_1 = \begin{cases} \dfrac{\pi}{2} - \theta & \text{if} \quad 0 < \theta \leq \dfrac{\pi}{2}, \\ \dfrac{3\pi}{2} - \theta & \text{if} \quad \dfrac{\pi}{2} \leq \theta \leq \dfrac{3\pi}{2},\ \theta \neq \pi, \\ \dfrac{5\pi}{2} - \theta & \text{if} \quad \dfrac{3\pi}{2} \leq \theta < 2\pi, \end{cases} \tag{58}$$

$$\beta_2 = \begin{cases} \pi - \theta & \text{if} \quad 0 \leq \theta \leq \pi,\ \theta \neq \dfrac{\pi}{2}, \\ 2\pi - \theta & \text{if} \quad \pi \leq \theta \leq 2\pi,\ \theta \neq \dfrac{3\pi}{2}. \end{cases} \tag{59}$$

Note that when θ vanishes or equals π in eqn. $(57)_1$ or θ equals $\pi/2$ or $3\pi/2$ in eqn. $(57)_2$, the integrals become hypersingular and retain a meaning only in the Hadamard sense. Therefore, in the limits $\theta \to 0$ or $\theta \to \pi$, eqn. $(57)_1$ reduces to

$$\begin{aligned} \tau_1^1 = \frac{\sin\phi}{2\pi^2 r} \Bigg\{ \Bigg[\int_0^\pi \left(\frac{\bar{b}\bar{\beta}\tan^2\alpha}{\Lambda(\alpha)} - \frac{1}{(\pi/2-\alpha)^2} \right) d\alpha - \frac{4}{\pi} \Bigg] \\ -[\bar{\gamma}(\bar{\mu}_3 + \bar{\gamma}) + \bar{\beta}(\bar{b} - \bar{\alpha})] \int_0^\pi \frac{\sin^2\alpha}{\Lambda(\alpha)} d\alpha \Bigg\}, \end{aligned} \tag{60}$$

while, when $\theta \to \pi/2$ or $\theta \to 3\pi/2$, eqn. $(57)_2$ reduces to

$$\begin{aligned} \tau_2^2 = \frac{\sin\phi}{2\pi^2 r} \Bigg\{ \Bigg[\int_0^\pi \left(\frac{\bar{a}\bar{\alpha}\tan^2\alpha}{\Lambda(\alpha+\pi/2)} - \frac{1}{(\pi/2-\alpha)^2} \right) d\alpha - \frac{4}{\pi} \Bigg] \\ -[\bar{\alpha}(\bar{a} - \bar{\beta}) + \bar{\gamma}(\bar{\mu}_3 + \bar{\gamma})] \int_0^\pi \frac{\sin^2\alpha}{\Lambda(\alpha+\pi/2)} d\alpha \Bigg\}, \end{aligned} \tag{61}$$

so that the integrals are regularized and correspond to Hadamard finite parts in the above eqns. (60) and (61).

4 Boundary element formulation

We consider here a homogeneously deformed nonlinear elastic solid, with a continuous and piecewise smooth boundary [Kellog (1953)], subjected to incremental tractions and displacements on prescribed parts of the boundary

$$v_i = \bar{v}_i \quad \text{on} \quad \partial B_v, \quad \text{and} \quad \tau_i = \bar{\tau}_i \quad \text{on} \quad \partial B_\tau. \tag{62}$$

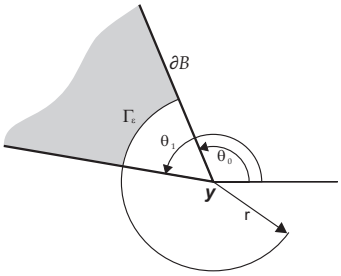

Figure 3: Angles θ_0 and θ_1 for a corner point $\mathbf{y}$.

The boundary integral equation for incremental displacements at a point $\mathbf{y}$ belonging to $\bar{B} = B \cup \partial B$, in the form obtained by Bigoni and Capuani (2002), is

$$C_i^g v_i(\mathbf{y}) = \int_{\partial B} \tau_i(\mathbf{x})\, v_i^g(\mathbf{x},\mathbf{y})\, dl_x - \fint_{\partial B} \tau_i^g(\mathbf{x},\mathbf{y})\, v_i(\mathbf{x})\, dl_x, \tag{63}$$

where C_i^g is the so-called $\mathbf{C}$-tensor defined such that:

- $\mathbf{C} = \mathbf{I}$, at internal points of B;
- $\mathbf{C} = \mathbf{I}/2$, at points on a smooth portion of the boundary ∂B;
- at corner points of a piecewise-smooth boundary:

$$C_i^g = \lim_{r \to 0} \int_{\theta_0}^{\theta_1} \tau_i^g(r,\theta) r d\theta, \tag{64}$$

where r and θ are polar coordinates centered at the corner point $\mathbf{y}$ and θ_0 and θ_1 are the angular coordinates of the half-tangents to the boundary at $\mathbf{y}$ (Fig. 3).

Note that the $\mathbf{C}$-tensor depends on material parameters, prestress state and geometry of the boundary. Values of the components of this tensor for a $\pi/2$–corner are listed in Table 1, for a Kirchhoff-Saint Venant material with $\lambda_0/\mu_0 = 2$, corresponding to $\nu = 0.333$ (the diagonal terms C_1^1 and C_2^2, both equal to 1/4, are not reported for conciseness). Different values of in-plane deviatoric prestress k and in-plane hydrostatic stress χ have been explored. As a consequence of the fact that the first Piola-Kirchhoff stress is unsymmetric, the $\mathbf{C}$-tensor results also unsymmetric, when the deviatoric prestress is different from zero.

Table 1: **C**-matrix for a Kirchhoff-Saint Venant material with $\lambda_0/\mu_0 = 2$. The collocation point **y** is set at a right-angle corner. Diagonal terms C_1^1 and C_2^2 are equal to $1/4$ from symmetry considerations.

$\chi = k$	C_2^1	C_1^2	$\chi = -k$	C_2^1	C_1^2
$k = 0.00$	0.11936	0.11936	$k = 0.00$	0.11936	0.11936
$k = 0.20$	0.11388	0.09196	$k = -0.20$	0.09196	0.11388
$k = 0.40$	0.10492	0.07074	$k = -0.40$	0.07074	0.10492
$k = 0.60$	0.09098	0.05265	$k = -0.60$	0.05265	0.09098
$k = 0.80$	0.06804	0.03499	$k = -0.80$	0.03499	0.06804
$k = 0.95$	0.03503	0.01722	$k = -0.95$	0.01722	0.03503

The boundary ∂B is discretized into elements Γ^e ($e = 1, \ldots, m$) of length l_e to arrive at a boundary element formulation. Within each element, the following representations are employed for incremental displacements and tractions

$$v_i = \varphi_p(\xi)\, \bar{v}_{ip}^e, \quad \tau_i = \varphi_p(\xi)\, \bar{\tau}_{ip}^e \qquad (p = 0, \cdots, \Theta), \tag{65}$$

where $\xi \in [0,1]$, $\bar{v}_{ip}^e$ and $\bar{\tau}_{ip}^e$ are, respectively, nodal incremental displacements and nominal tractions, φ_p are Lagrange polynomial shape functions of degree Θ ($\Theta = 1$ in the applications) and the repeated index p is to be summed between 0 and Θ. Employing representation (65) and collocating the point **y** at $\mathbf{y}^{(\bar{e},\bar{p})}$, corresponding to the node $\bar{p}$ of the element $\bar{e}$, the boundary integral equation (63) can be discretized as

$$C_i^g \bar{v}_{i\bar{p}}^{\bar{e}} + \sum_{e=1}^{m} \bar{v}_{ip}^e \int_{\Gamma_e} \varphi_p(\xi) \tau_i^g(\mathbf{x}(\xi), \mathbf{y}^{(\bar{e},\bar{p})}) dl_\xi = \sum_{e=1}^{m} \bar{\tau}_{ip}^e \int_{\Gamma_e} \varphi_p(\xi) v_i^g(\mathbf{x}(\xi), \mathbf{y}^{(\bar{e},\bar{p})}) dl_\xi. \tag{66}$$

Eqn. (66) is then collocated at the m nodes along the two directions x_1 and x_2, leading to an algebraic system of $2m$ equations in $2m$ unknowns.

5 Applications and numerical results

The main purpose of this Section is to test the validity of the boundary element formulation on problems of prestressed elastic compressible solids. Before presenting these applications, however, a digression is instrumental on the analysis of shear band formation using the perturbative approach proposed by Bigoni and Capuani (2002), which has never previously been used for *compressible* materials.

5.1 Perturbative approach to shear band formation

Following the traditional approach [Rice (1977)], the formation of shear bands can be considered as the emergence of discontinuous strain rate patterns, which become possible when the boundary of the elliptic regime is reached. When this occurs, two situations become possible:

- at the EI/P boundary shear bands are always aligned parallel to the tensile axis for uniaxial traction and orthogonal to the compressive direction for uniaxial compression;
- at the EC/H boundary two shear bands become possible, equally inclined with respect to the principal axes of prestress at an angle ς between the x_1–axis and the shear band plane, solution of

$$\tan\varsigma = \pm\sqrt{\frac{2\bar{a}\bar{\alpha}-\bar{d}}{2\bar{b}\bar{\beta}-\bar{d}}}. \tag{67}$$

Using solution (40), a perturbative approach to localized deformations can be pursued, following the Bigoni and Capuani (2002) proposal. In fact, since the incremental problem is linear, several loading systems can be constructed by superimposing the unit force solution (40). We consider in this Section a dipole in an infinite prestressed medium, which is the simplest self-equilibrated perturbation. In particular, we consider two equal and opposite unit incremental forces acting at a distance $2l$ and inclined of an angle ε (positive in the counterclockwise sense) with respect to the principal axis of prestress x_1. The modulus of the incremental displacement field may be easily evaluated by superposition, using eqns. (40).

Level sets of the modulus of incremental displacement $|\mathbf{v}|$ are reported in Fig. 4 for a Kirchhoff–Saint Venant material with $\lambda_0/\mu_0 = 2$ (corresponding to $\nu = 0.333$, see Section 2.3 and Fig. 1), and a dipole inclined at angles $\varepsilon = 0$, $\varepsilon = \pi/4$, and $\varepsilon = \pi/2$ with respect to the x_1–axis. Three values of uniaxial compressive prestress in the direction of the x_2–axis have been considered, namely, $k = 0.55$ (close to the EC/H boundary), $k = 0.37$, and $k = 0$.

An examination of Fig. 4 and a comparison with analogous results relative to incompressible elasticity [Bigoni and Capuani (2002)] reveals that volumetric compressibility does not introduce qualitative changes and that the perturbative approach correctly predicts the shear band onset and directional properties.

5.2 Numerical results

The boundary element formulation developed in the previous sections has been implemented into a Fortran 90 code and tested for different boundary value problems.

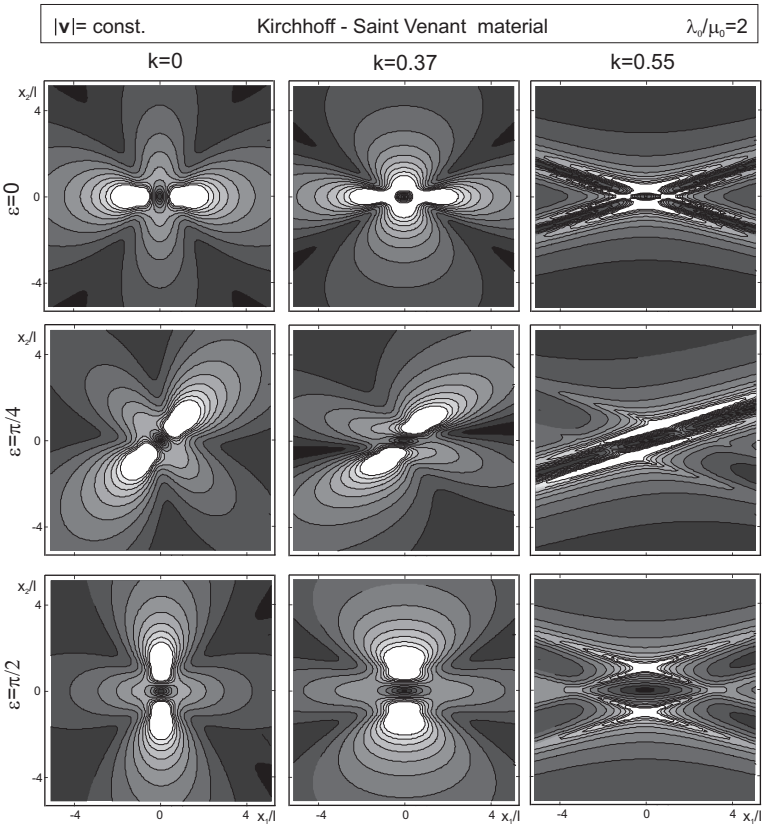

Figure 4: Level sets of the modulus of the incremental displacement for a dipole oriented at an angle ε with respect to the principal axis of prestress x_1, for a Kirchhoff-Saint Venant material ($\lambda_0/\mu_0 = 2,\ \nu = 0.333$, see Fig. 1 for the classification of regimes of this material), at different level of compressive prestress. The inclination of bands visible when the prestress is near the EC/H boundary, $k = 0.55$, agrees well with that predicted by eqn. (67), $\varsigma = 16^\circ 49$.

Linear shape functions have been adopted for incremental displacements and tractions at the boundary and integrals have been numerically computed by standard Gauss quadrature rules.

We consider in the following deformations of elastic blocks subject to uniaxial stress and incrementally loaded i.) under shear and ii.) by symmetric and antisymmetric perturbations, to reveal the onset of bifurcations in diffuse modes.

5.2.1 Square elastic block under simple shear deformation

The first example consists of a square, elastic, orthotropic block of edge $2b$, constrained to homogeneous plane deformations, subject to an incremental nominal shear stress τ_{21} applied to the upper edge (Fig. 5).

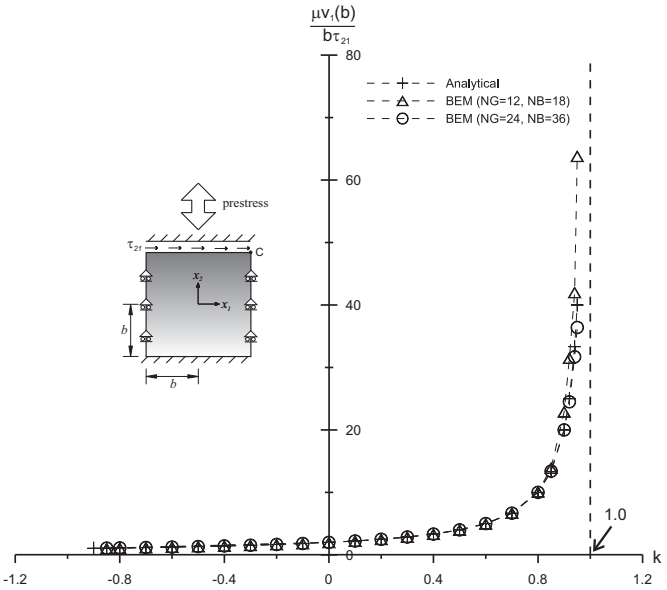

Figure 5: Simple shear deformation of an elastic block: dimensionless incremental displacement of the corner point C versus prestress k. The numerical solution, obtained with different numbers of Gauss nodes for Green's functions (NG) and for the boundary integral equations (NB), is compared with the analytical one, eqn. (68).

A uniaxial state of prestress with principal directions aligned parallel to the edges of the block is prescribed in terms of the non-dimensional parameters k and χ, the latter taken equal to $-k$, so that σ_1 is always null, while the block is subjected to compression ($k > 0$) or tension ($k < 0$) aligned parallel to the x_2-direction. The analytical solution is known for this simple boundary value problem [see Bigoni, Capuani, Bonetti and Colli (2007)] and can be written as

$$v_1(x_2) = \frac{(x_2 + b)\tau_{21}}{\mu(1-k)}, \quad v_2 = 0. \tag{68}$$

Note that the solution (68) does not involve the material parameters μ_1, μ_2 and

μ_3, so that it remains valid for every μ and for $k \neq 1$. In the limit $k \to 1$ the material becomes vanishing stiff in the horizontal direction and the corresponding displacement tends to infinity, so that a horizontal strain discontinuity (shear band) becomes possible.

The numerical solution has been compared with the analytical one, eqn. (68), adopting a uniform mesh of 72 boundary elements. Results in terms of non-dimensional horizontal displacement of point C versus prestress parameter k are displayed in Fig. 5. The number of Gauss points used for integrations of Green's functions (NG) and of boundary equations (NB) has been varied from 12-18 to 24-36, respectively. In the latter case the numerical accuracy is higher, especially in proximity of the parabolic boundary, which occurs at $k = 1$ ($k = -1$) in compression (in tension). It can be concluded that the numerical procedure is quite accurate, but the numerical precision decreases for increasing k, so that the number of Gauss points has to be increased to get results with comparable accuracy.

5.2.2 Bifurcation of a square elastic block

Loss of uniqueness is investigated in the incremental response of a uniaxially prestressed square (in the current configuration) elastic block under plane-strain conditions ($\lambda_3 = 1$, $J = \lambda_1\lambda_2$), made up of compressible Mooney-Rivlin material (see Section 2.4). In particular, we prescribe a homogeneous uniaxial compression σ_2 along the x_2–axis ($\sigma_2 < 0$), so that by imposing the vanishing of tractions on the lateral free sides ($\sigma_1 = 0$), a relation between the in-plane stretches λ_1 and λ_2 can be derived, namely

$$c_1 c_3 J^{2/3}(2\lambda_1^2 - \lambda_2^2 - 1) + 3J^{7/3}(J-1) + c_2 c_3(\lambda_1^2 - 2\lambda_2^2 + J^2) = 0, \tag{69}$$

from which, for a given λ_2, the value of λ_1 can be evaluated, thus providing the prestrain/prestress state.

Antisymmetric (and symmetric) bifurcations from this state are analyzed with our BE code applying an antisymmetric (symmetric) perturbation load (τ in Figs. 6 and 7) on small portions of the lateral edges equal, respectively, to 1/6 and 2/9 of the total edge length. A coarse integration with NG=12 and NB=18 and a fine integration with NG=24 and NB=36 have been adopted. The latter gives a much better agreement with an exact analysis (reported in Appendix B and predicting an antisymmetric mode for $k \simeq 0.416$ and a symmetric mode for $k \simeq 0.595$) and with the numerical solution obtained with the commercial code ABAQUS-Standard (Ver. 6.5–ABAQUS Inc., Providence, RI), as evidenced in Figs. 6 and 7.

In Figs. 6 and 7 the dimensionless horizontal incremental displacement of a representative point of each problem (denoted with letter A) is plotted versus the prestress k. It is clear that the stiffness in the incremental response varies significantly

as a function of k. In particular, whereas a tensile prestress ($k < 0$) increases the stiffness in the incremental problem, a compression state (corresponding to positive values of k) induces stiffness degradation, as can be inferred from the deformed shapes of the lateral edges shown in Figs. 8 and 9 for three different values of k, obtained at constant incremental load τ. This degradation becomes dramatic when a critical value of k is reached, beyond which the stiffness becomes negative.

The numerical results obtained with our BE code are compared with the results obtained with ABAQUS employing four-noded plane-strain quadrilateral elements (CPE4) in Figs. 8 and 9. For the antisymmetric mode, results are in excellent agreement, even when the bifurcation stresses $k = 0.413$ and $k = 0.595$ are approached. In both cases the qualitative deformations are similar for every value of k, and the incremental displacements tend to blow up when the bifurcation point is approached.

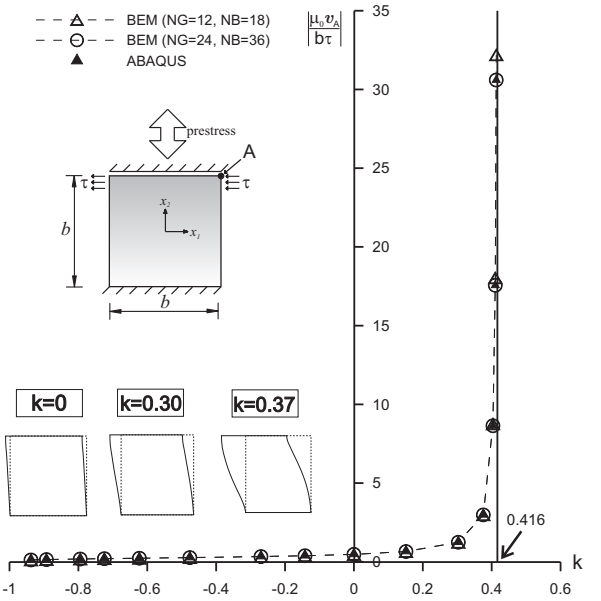

Figure 6: Dimensionless horizontal incremental displacement of point A versus prestress k for antisymmetric perturbations of a compressible Mooney-Rivlin square block prestressed under uniaxial tension/compression. NG: number of Gauss nodes employed in the integration of the Green's function; NB: number of Gauss nodes employed in the integration of the boundary integral equation. The asymptote in the graph corresponds to the first antisymmetric bifurcation mode, occurring at $k = 0.416$ and calculated with the analysis reported in Appendix B.

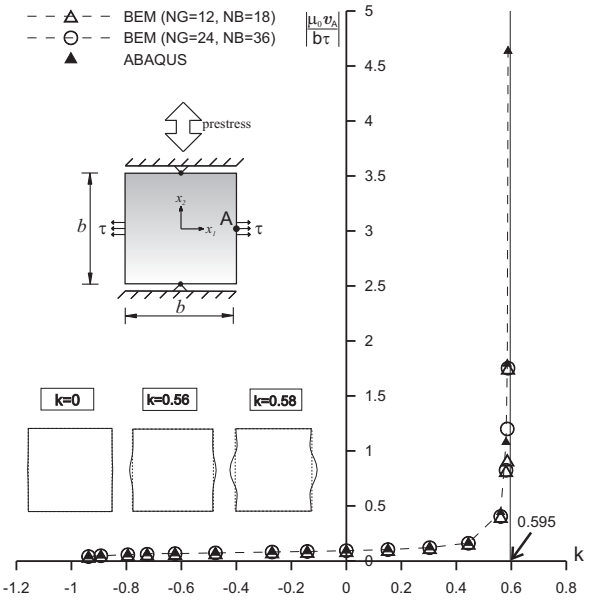

Figure 7: Dimensionless horizontal incremental displacement of point A versus prestress k for symmetric perturbations of a compressible Mooney-Rivlin square block prestressed under uniaxial tension/compression. NG: number of Gauss nodes employed in the integration of the Green's function; NB: number of Gauss nodes employed in the integration of the boundary integral equation. The asymptote in the graph corresponds to the first symmetric bifurcation mode, occurring for $k = 0.595$ and calculated with the analysis reported in Appendix B.

Finally, different results pertaining to the antisymmetric perturbation are reported in Fig. 10, for a Mooney-Rivlin material with decreasing values of the ratio $\nu = \{0, 0.18, 0.32, 0.40, 0.50\}$ (corresponding to $\mu_0/q_0 = \{3/2, 4/5, 2/5, 1/5, 0\}$), are shown. It is evident that the critical value of k increases with the increase of the ratio ν. In the limit of incompressibility, $\nu = 0.5$, the critical stress approaches that obtained for incompressible Mooney-Rivlin model [Brun, Capuani, Bigoni (2003b)].

5.2.3 *Bifurcations of a rectangular elastic block at different aspect ratios and comparison with the Euler buckling model*

The critical buckling stress for an elastic block of compressible Mooney-Rivlin material (again under plane-strain conditions) is investigated in this Section for different values of aspect ratio, l/b in Fig. 11. Three different loading and constraint

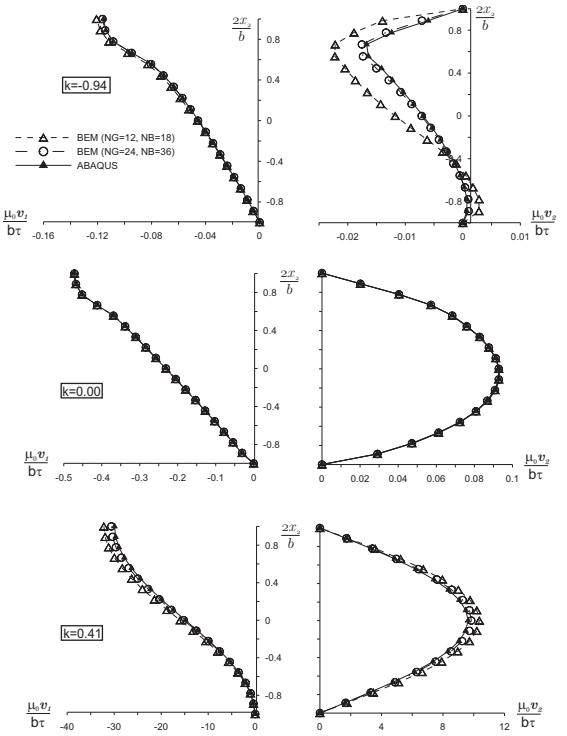

Figure 8: Profiles of the dimensionless incremental displacement components of the vertical edge of the square compressible Mooney-Rivlin block (Fig. 6), for different values of prestress parameter k. Left: component v_1; right: component v_2. The bifurcation load corresponds to $k \simeq 0.416$.

schemes are considered, as represented in Fig. 11, where the qualitative deformations obtained with our numerical code near bifurcation are reported for $l/b = 2$.

Results in terms of the dimensionless critical prestress $|\sigma_2^b|/\mu_0$ versus the aspect ratio l/b are reported in Fig. 12 for $\nu = 0.32$ ($\mu_0/q_0 = 2/5$). Numerical results obtained with our BE code are compared with the corresponding approximate solutions obtained with the Euler buckling model, i.e.

$$\frac{|\sigma_2^b|}{\mu_0} = \frac{\pi^2}{6(1-\nu)} \left(\frac{b}{l_0}\right)^2, \tag{70}$$

where l_0 is the 'effective length', respectively equal to l, $2l$, $l/\sqrt{2}$ for the first, second and third case. Furthermore, an analytical solution of a situation very similar to

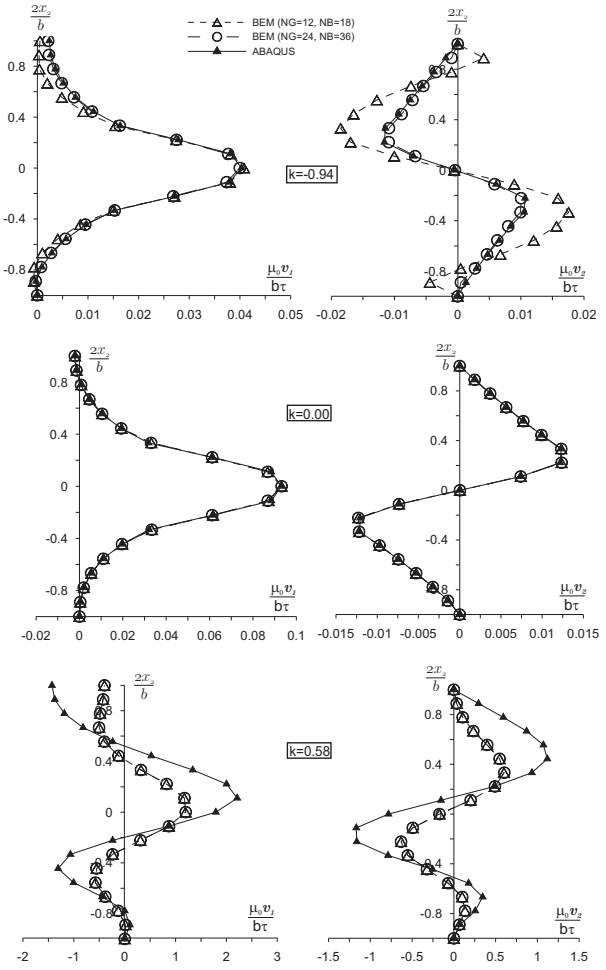

Figure 9: Profiles of the dimensionless incremental displacement components of the vertical edge of the square compressible Mooney-Rivlin block (Fig. 7), for different values of prestress parameter k. Left: component v_1; right: component v_2. The bifurcation load corresponds to $k \simeq 0.595$.

case 1, namely, two rigid smooth constraints at the upper and lower face is provided (deferred to Appendix B).

It can be observed that for high aspect ratios l/b, in other words for slender elastic blocks, the values obtained with our BE code are in good agreement with those predicted by the Euler model. However, the Euler model becomes inaccurate for

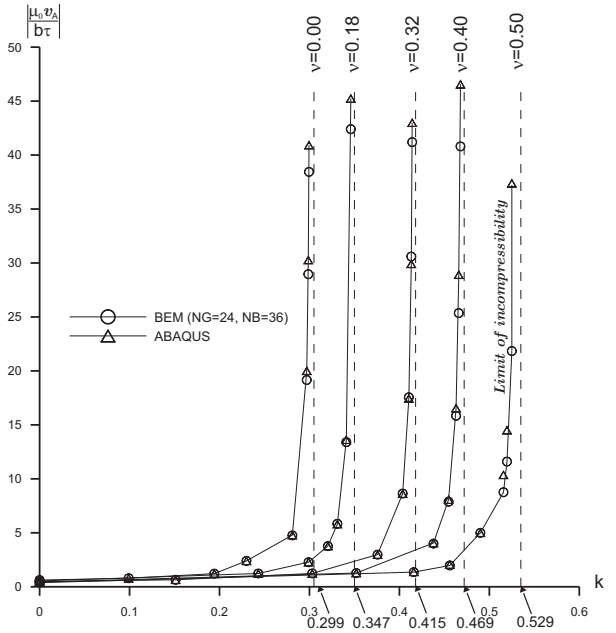

Figure 10: Dimensionless incremental displacement of the corner point A versus prestress k for an antisymmetric perturbation (geometry of Fig. 6), for different values of the ratio ν for compressible Mooney-Rivlin solid.

low ratios l/b and a numerical approach is mandatory to study the instability of thick specimens under different constraint conditions (the analytical solution is only available for the constraints of infinite normal stiffness and free tangential sliding, the so-called 'case 1'). Our boundary element approach becomes now a useful tool to compute the buckling loads for thick elastic blocks. In particular, the limit $l/b \to 0$ for case 1 corresponds to surface instability stress, as checked with the analytical solution reported in Appendix B. For cases 2 and 3, the approached values for $l/b \to 0$ are lower than that for case 1 and strongly depend on the boundary conditions of the specimen (Fig. 11) which provide a different constraint to the block. However, caution should be exercised in the interpretation of numerical results for very low values of l/b.

6 Conclusions

Infinite-body Green's functions for incremental displacements, displacement gradients, nominal stresses and tractions have been derived for a uniformly prestressed

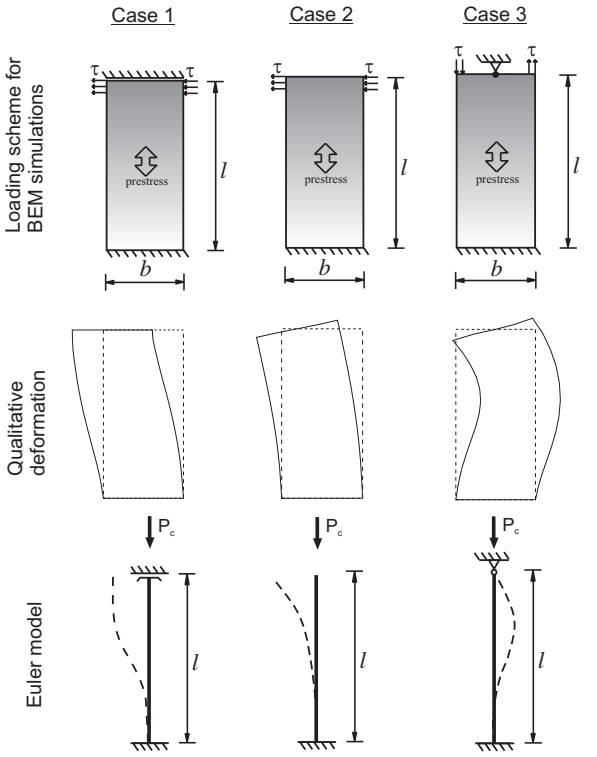

Figure 11: Loading and constraint schemes for the numerical simulations of Fig. 12, qualitative deformations near the bifurcation load for $l/b = 2$ and corresponding Euler buckling modes.

and prestrained nonlinear *compressible* elastic solid. From these singular solutions and relevant boundary integral equations, a boundary element technique has been developed to analyze incremental problems of nonlinear elastic deformations. When the incremental deformation is superimposed upon a uniform state, the formulation does not involve any volume integral (with the possible exception when body forces are present) and yields an elegant and efficient numerical tool useful in the analysis of bifurcation loads and modes, including shear bands.

The extension of the proposed approach to nonuniform ground fields has not been addressed, but can be certainly pursued through a generalization of the technique proposed by Bertoldi, Brun and Bigoni (2005), therefore opening the way to a new boundary element approach for nonlinear elastic deformations.

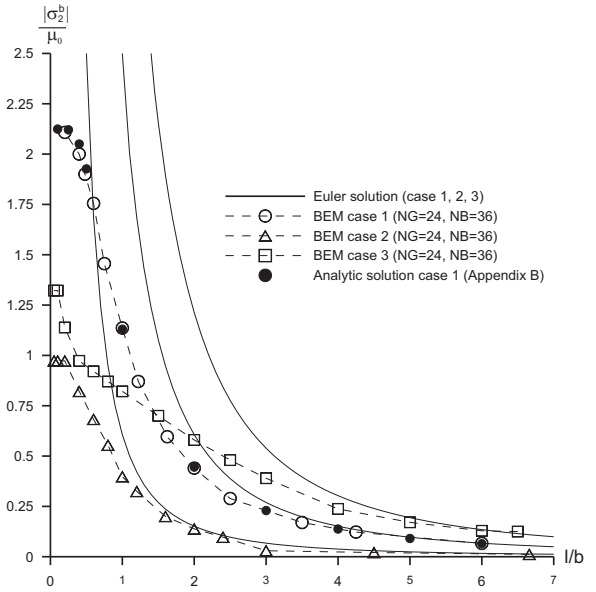

Figure 12: Dimensionless buckling load $|\sigma_2^b|/\mu_0$ versus aspect ratio l/b for an elastic block of compressible Mooney-Rivlin material with $\nu = 0.32$. Numerical results obtained with the BE code for the three cases of Fig. 11 are compared with the corresponding buckling loads obtained with the Euler formula (70). For case 1, results obtained from the exact analysis developed in Appendix B are reported.

Acknowledgement: The financial support of PRIN grant n. 2007YZ3B24 'Multi-scale Problems with Complex Interactions in Structural Engineering', financed by Italian Ministry of University and Research is gratefully acknowledged.

References

Balas, J.; Sladek, J.; Sladek, V. (1989): *Stress Analysis by Boundary Element Methods*. Elsevier, Amsterdam.

Bertoldi, K.; Brun, M.; Bigoni, D. (2005): A new boundary element technique without domain integrals for elastoplastic solids. *International Journal for Numerical Methods in Engineering*, vol. 64, pp. 877-906.

Bigoni, D.; Capuani, D. (2002): Green's function for incremental nonlinear elasticity: shear bands and boundary integral formulation. *Journal of the Mechanics and Physics of Solids,* vol. 50, pp. 471-500.

Bigoni, D.; Capuani, D. (2005): Time-harmonic Green's function and boundary

integral formulation for incremental nonlinear elasticity: dynamics of wave patterns and shear bands. *Journal of the Mechanics and Physics of Solids,* vol. 53, pp. 1163-1187.

Bigoni, D.; Capuani, D.; Bonetti, P.; Colli, S. (2007): A novel boundary element approach to time-harmonic dynamics of incremental non-linear elasticity: the role of prestress on structural vibrations and dynamic shear banding. *Computer Methods in Applied Mechanics and Engineering,* vol. 196, pp. 4222-4249.

Bigoni, D.; Gei, M.; Movchan, A.B. (2008): Dynamics of a prestressed stiff layer on an elastic half space: filtering and band gap characteristics of periodic structural models derived from long-wave asymptotics. *Journal of the Mechanics and Physics of Solids,* vol. 56, pp. 2494-2520.

Biot, M.A. (1965): *Mechanics of Incremental Deformations*. J. Wiley and Sons, New York.

Brun, M.; Capuani, D.; Bigoni, D. (2003a): A boundary element technique for incremental, nonlinear elasticity. Part I: formulation. *Computer Methods in Applied Mechanics and Engineering,* vol. 192, pp. 2461-2479.

Brun, M.; Capuani, D.; Bigoni, D. (2003b): A boundary element technique for incremental, nonlinear elasticity. Part II: bifurcation and shear bands. *Computer Methods in Applied Mechanics and Engineering,* vol. 192, pp. 2481-2499.

Ciarlet, P.G. (1988): *Mathematical Elasticity. Vol. I: Three-Dimensional Elasticity.* North-Holland, Amsterdam.

Courant, R.; Hilbert, D. (1962): *Methods of Mathematical Physics, Vol. II*. Wiley, New York.

Cruse, T.A. (1988): *Boundary Elements Analysis in Computational Fracture Mechanics*. Kluwer, Dordrecht.

DeBotton, G.; Tevet-Deree, L.; Socolsky, E.A. (2007): Electroactive heterogeneous polymers: analysis and applications to laminated composites. *Mechanics of Advanced Materials and Structures,* vol. 14, pp. 13-22.

Gaul, L.; Kögl, M.; Wagner, M. (2003): *Boundary Elements Methods for Engineers and Scientists. An Introductory Course with Advanced Topics*. Springer.

Gei, M. (2008): Elastic waves guided by a material interface. *European Journal of Mechanics-A/Solids*, vol. 27, pp. 328-345.

Gei, M.; Movchan, A.B.; Bigoni, D. (2009): Band-gap shift and defect-induced annihilation in prestressed elastic structures. *Journal of Applied Physics*, vol. 105, 063057.

Gel'fand, I.M.; Shilov, G.E. (1964): *Generalized Functions, Vol. 1, Properties and Operations*. Academic Press, New York.

Hill, R. (1979): On the theory of plane strain in finitely deformed compressible materials. *Mathematical Proceedings of Cambridge Philosophical Society,* vol. 86, pp. 161-178.

Kellog, O.D. (1953): *Foundations of Potential Theory*. Dover, New York.

Maier, G. (1983): On elastoplastic analysis by boundary elements. *Mechanics Research Communications*, vol. 10, pp. 45-52.

Mantic, V.; Paris, F. (1998): Integral kernels in the 2D Somigliana displacement and stress identities for anisotropic materials. *Computational Mechanics*, vol. 22, pp. 77-87.

Michel, J.C.; Lopez-Pamies, O.; Ponte Castañeda, P.; Triantafyllidis, N. (2007): Microscopic and macroscopic instabilities in finitely strained porous elastomers. *Journal of the Mechanics and Physics of Solids,* vol. 55, pp. 900-938.

Miers, L.S.; Telles, J.C.F. (2004): A general tangent operator procedure for implicit elastoplastic BEM analysis. *CMES: Computer Modeling in Engineering & Sciences*, vol. 6, pp. 431-439.

Mukherjee, S. (1977): Corrected boundary integral equations in planar thermoplasticity. *International Journal of Solids and Structures,* vol. 13, pp. 331-335.

Ogden, R.W.; Roxburgh, D.G. (1994): Stability and vibration of prestressed compressible elastic plates. *International Journal of Engineering Sciences,* vol. 32, pp. 427-454.

Plante, J.S.; Dubowsky, S. (2006): Large-scale failure modes of dielectric elastomer actuators. *International Journal of Solids and Structures,* vol. 43, pp. 7727-7751.

Rice, J.R. (1977): The localization of plastic deformation. In Koiter, W.T. (ed.), *Theoretical and Applied Mechanics*. North-Holland, Amsterdam, pp. 207-220.

Shiah, Y.C.; Lin, Y.C.; Tan, C.L. (2006): Boundary element stress analysis of thin layered anisotropic bodies. *CMES: Computer Modeling in Engineering & Sciences*, vol. 16, pp. 15-26.

Sladek, V., Sladek, J. (1999) Displacement gradients in BEM formulation for small strain plasticity. *Engineering Analysis with Boundary Elements*, vol. 23, pp. 471-477.

Stafford, C.M.; Harrison, C.; Beers, K.L.; Karim, A.; Amis, E.J.; Vanlandingham, M.R.; Kim, K.C.; Volksen, W.; Miller, R.D.; Simonyi, E.E. (2004): A buckling-based metrology for measuring the elastic moduli of polymeric thin films. *Nature Materials*, vol. 3, pp. 545-550.

Swedlow, J.L.; Cruse, T.A. (1971): Formulation of boundary integral equations for three dimensional elastoplastic flow. *International Journal of Solids and Struc-*

tures, vol. 7, pp. 1673-1683.

Telles, J.C.F. (1983): *The boundary element method applied to inelastic problems*. Springer, Berlin.

Vogel, S.M.; Rizzo, F.J. (1973): An integral equation formulation of three dimensional anisotropic elastostatic boundary value problems. *Journal of Elasticity,* vol. 3, pp. 1-14.

Appendix A. On singular integrals in eqns. $(54)_{1,2}$

By noting that

$$\oint_{|\boldsymbol{\omega}|=1} \frac{n_1}{\omega_1}\frac{d\omega}{\boldsymbol{\omega}\cdot\mathbf{x}} = \frac{n_1}{r}\int_0^{2\pi} \frac{d\alpha}{\cos\alpha\cos(\alpha+\theta)} = 0, \tag{A.1}$$

and assuming (53), eqn. $(52)_1$ can be written as

$$\begin{aligned}\tau_1^1 = \frac{1}{2\pi^2 r}\int_0^{\pi} \frac{\cos\alpha\cos\phi+\sin\alpha\sin\phi}{\cos\alpha\,\Lambda(\alpha+\theta)}\{\bar{b}\bar{\beta}\tan(\alpha+\theta)\\ -[\bar{\gamma}(\bar{\mu}_3+\bar{\gamma})+\bar{\beta}(\bar{b}-\bar{\alpha})]\sin(\alpha+\theta)\cos(\alpha+\theta)\}\,d\alpha.\end{aligned} \tag{A.2}$$

As factor multiplying $\cos\phi$ vanishes in eqn. (A.2), we obtain the form $(54)_1$ of the incremental traction.

Let us consider now eqn. $(52)_2$ and note that

$$\oint_{|\boldsymbol{\omega}|=1} \frac{n_2}{\omega_2}\frac{d\omega}{\boldsymbol{\omega}\cdot\mathbf{x}} = \frac{n_2}{r}\int_0^{2\pi} \frac{d\alpha}{\cos\alpha\sin(\alpha+\theta)} = 0. \tag{A.3}$$

Hence, we can write

$$\begin{aligned}\tau_2^2 = -\frac{1}{2\pi^2 r}\int_0^{\pi} \frac{\cos\alpha\cos\phi+\sin\alpha\sin\phi}{\cos\alpha\,\Lambda(\alpha+\theta)}\{\bar{a}\bar{\alpha}\cot(\alpha+\theta)\\ -[\bar{\gamma}(\bar{\mu}_3+\bar{\gamma})+\bar{\alpha}(\bar{a}-\bar{\beta})]\sin(\alpha+\theta)\cos(\alpha+\theta)\}\,d\alpha,\end{aligned} \tag{A.4}$$

and, since the factor multiplying $\cos\phi$ vanishes in eqn. (A.4), we obtain the form $(54)_2$ of the incremental traction.

Appendix B. Diffuse bifurcations of a homogeneously deformed, compressible, elastic layer

Diffuse bifurcations are investigated of an elastic rectangular block ($-b/2 \le x_1 \le b/2$; $-l/2 \le x_2 \le l/2$), subject to a homogenous compressive uniaxial stress (σ_2) along the direction x_2, constrained with two smooth rigid plates at $x_2 = \pm l/2$. The

Table 2: Critical stretch λ_2 and dimensionless prestress k at bifurcation for a Mooney-Rivlin block in plane-strain uniaxial compression for different values of ratio ν for antisymmetric and symmetric modes.

ν	λ_2, k (antisymm. mode)	λ_2, k (symm. mode)
0.18	0.7065, 0.7011	0.5894, 0.8531
0.32	0.7216, 0.4152	0.5664, 0.5952
0.40	0.7321, 0.4678	0.5319, 0.7395

equilibrium equations (9) for a generic compressible material still hold true. Bifurcation of equilibrium is detected by considering, for the incremental displacement, the form

$$v_j = A_j e^{mx_1} e^{inx_2} \quad (j = 1,2), \tag{B.1}$$

where n is the wavenumber of the bifurcation mode and m a parameter to be determined. For the antisymmetric mode, the first bifurcation corresponds to $n = \pi/b$, whereas for the symmetric mode $n = 2\pi/b$. Introducing the form (B.1) into eqns. (9) we obtain a homogenous system

$$\begin{bmatrix} \bar{a}m^2 - \bar{\beta}n^2 & i(\bar{\mu}_3 + \bar{\gamma})nm \\ i(\bar{\mu}_3 + \bar{\gamma})nm & \bar{\alpha}m^2 - \bar{b}n^2 \end{bmatrix} \begin{bmatrix} A_1 \\ A_2 \end{bmatrix} = \begin{bmatrix} 0 \\ 0 \end{bmatrix}, \tag{B.2}$$

which admits non trivial solutions only if the determinant of the coefficient matrix vanishes. The characteristic equation governing the equilibrium at the bifurcation thus is

$$\bar{a}\bar{\alpha}m^4 + \bar{d}n^2m^2 + \bar{b}\bar{\beta}n^4 = 0, \tag{B.3}$$

which provides four solutions m_p $(p = 1,\ldots,4)$, so that the general solution in terms of displacements can be written as a linear combination of the four eigenvectors $[A^p]$ $(p = 1,\ldots,4)$ associated with m_p as

$$v_j = \sum_{p=1}^{4} A_j^p e^{m_p x_1} e^{inx_2} \quad (j = 1,2). \tag{B.4}$$

The boundary conditions for a rectangular block with smooth constraints at $x_2 = \pm l/2$ imply that along the free vertical edges the nominal incremental traction is null, namely,

$$\dot{t}_{11} = 0, \quad \dot{t}_{21} = 0 \quad (x_1 = \pm b/2), \tag{B.5}$$

which, substituting eqn. (B.4) in the constitutive eqns. (5) and exploiting the relationship between amplitudes A_1^p and A_2^p given by $(B.2)_1$

$$A_2^p = A_1^p \frac{i(\bar{a}m_p^2 - \bar{\beta}n^2)}{(\bar{\mu}_3 + \bar{\gamma})nm_p}, \tag{B.6}$$

can be rewritten in a compact form as

$$[M][A_1^p] = [0], \tag{B.7}$$

where $[M]$ is a coefficient matrix and $[A_1^p]^T = [A_1^1\ A_1^2\ A_1^3\ A_1^4]$. The critical value for the stretch λ_2 (under assumption of uniaxial state of stress in the x_2 direction) is finally obtained by imposing the vanishing of $\det[M]$.

For a compressible Mooney-Rivlin material bifurcations are only possible in compression ($k > 0$), so that for $\nu = 0.32$ ($\mu_0/q_0 = 2/5$), the first bifurcation is an antisymmetric mode (Fig. 6), occurring at $k \simeq 0.415$, while a symmetric mode (Fig. 7) is detected at $k \simeq 0.595$. Different values of critical stretch λ_2 and dimensionless prestress k as functions of the constitutive parameters for a Mooney-Rivlin material are shown in Table 2.